IERCU

Institute of Economic Research, Chuo University
50th Anniversary Special Issues

Dynamics in Delay IS-LM Model with Tax Collections

Akio Matsumoto	Ferenc Szidarovszky
Chuo University	University of Pécs

September 2013

INSTITUTE OF ECONOMIC RESEARCH

Chuo University

Tokyo, Japan

Dynamics in Delay IS-LM Model with Tax Collections*

Akio Matsumoto   Ferenc Szidarovszky
Chuo University†   University of Pécs‡

Abstract

An IS-LM model is developed for the dynamics of income, interest rate and money stock with delay in tax revenue. The main aim is to show that the delay matters in macro dynamics. Two different delays, fixed time delays and continuously distributed time delays, are considered explicitly and described by delay-differential equations and integro-differential equations, respectively. Conditions for the local stability of the two models are derived and compared. The destabilizing effects caused by the delay are numerically examined. Emergence of wide spectrum of dynamics ranging from simple cyclic oscillations to complex dynamics involving chaos is described through Hopf bifurctions.

Keywords: Fixed time delay, Continuously distributed time delay, Hopf bifurcation, Stability switch, IS-LM model

JEL number: E12, E32, E37, E62

1 Introduction

Since the pioneering work of Kalecki (1935) and the seminal work of Goodwin (1951), it has been recognized that economic dynamic systems usually incorporate delays in their actions and delay is one of the essentials for macroeconomic fluctuation. Nevertheless, little attention has been given to studies on delay in economic variables over the past few decades. After a long "gestation" period of time, however, the number of studies on delay gradually increases and various attempts have been done on the impact of delays on macro dynamics.[1] Among others, we draw attention to the papers of De Cesare and Sportelli (2005) and Fanti and Manfredi (2007), (DS and FM henceforth) and re-examine the stability/instability effects caused by a delay in the tax collection from a slightly different point of view. Both papers introduce time delay into a simple IS-LM model with a pure money financing deficit, which are used to show the existence of cyclic fluctuations of the macro variables (Schinasi (1981, 1982) and Sasakura (1994)). Noticing the established fact that there are delays in collecting tax, DS concerns "economic situations where a finite time delay cannot be ignored" and investigates how the fixed time delay (fixed delay henceforth) in tax collection affects the fiscal policy outcomes. Two results are shown: the emergence of limit cycle through Hopf bifurcation when the length of the delay becomes longer and the co-existence of multiple stable and unstable limit cycles when the steady (equilibrium) point is locally stable. On the other hand, FM replaces the fixed time delay with the continuously distributed time delay (distributed delay henceforth), emphasizing the evidence that there is "a wide variation in collection lag" and demonstrates the possibility that in the same IS-LM framework, complex dynamics involving chaos is born through an *ála* period-doubling bifurcation with respect to the length of the delay.

The purpose of this paper is to further explore what dynamics the delay IS-LM model can generate.[2] Specifying some of parameters, we analytically and numerically examine delay effects caused by changing the length of delay and tax effects caused by changing the value of the tax coefficient to show that "delay really matters." The followings are demonstrated:

---

[1] In the literature of time delay, there are two different modeling ways in continuous-time scale: fixed time delay and continuously distributed time delay The former is applicable when an institutionally or socially determined fixed period of time delay is presented for the agents involved. The latter is appropriate for economic situations in which different lengths of delays are distributed over heterogeneous agents or the length of the delay is random depending on unforeseeable circumstance. The choice of the type of delay has situation-dependency and results in the use of different analytical tools. In the cases of fixed time delay, dynamics is described by a delay differential equation whose characteristic equation is a mixed polynomial-exponential equation with infinitely many eigenvalues. In the cases of continuously distributed time delay, Volterra-type integro-differential equations are used to model the dynamics and with appropriate weighting function their characteristic equations have finitely many eigenvalues. A comprehensive summary of the theory of fixed delays is given in Bellman and Cooke (1956), and the mathematical methodology of dealing with distributed delays is presented in Cushing (1977).

[2] In Matsumoto and Szidarovszky (2013), we unify these two models and consider dynamics in an IS-LM model augmented with both fixed and distributed delays.

(I) A fixed delay IS-LM model can generate not only cyclic fluctuations which are qualitatively different from those in the non-delay model but also complex dynamics;

(II) Comparing the distributed model with the fixed model reveals that the distributed model is more stable than the fixed model in the sense that the former has a larger stable region than the latter;

(III) An increase of the shape parameter of the weighting function of the distributed model has a destabilizing effect by decreasing the stability region;

(IV) If the shape parameter converges to infinity, then the stability region converges to that of the fixed delay model.

This paper develops as follows. In Section 2, the fixed delay in tax collection is introduced and the delay and tax effects are examined. In Section 3, the fixed delay is replaced with the distributed delay. After conducting stability analysis, we numerically show that stability is sensitive to the shape of the delay kernel and analytically show that the distributed model converges to the fixed model when the delay kernel tends to the Direc delta function. Section 4 offers conclusions and further research directions.

2 Fixed Delay IS-LM Model

As a benchmark for macro stability analysis, we start with a non-delay IS-LM model with a pure money financing deficit:

$$
(M_N): \begin{cases} \dot{Y}(t) = \alpha \left[I(Y(t), R(t)) - s\left(Y(t) - T(t)\right) + g - T(t) \right], \\[2mm] \dot{R}(t) = \beta \left[L(Y(t), R(t)) - M(t) \right], \\[2mm] \dot{M}(t) = g - T(t), \end{cases}
$$

where the three state variables, Y, R and M, respectively represent income, interest rate and real money supply, the parameters, a, β, g and s are positive adjustment coefficients in the markets of income and money, constant government expenditure and the constant marginal propensity to save and $I(\cdot)$ and $L(\cdot)$ denote the investment and liquidity preference functions. Tax revenue is denoted by T and is collected as a lump sum with a constant rate, $0 < \tau < 1$,

$$
T(t) = \tau Y(t). \tag{1}
$$

Following DS, we specify the investment and money demand functions as

$$
I(Y, R) = A\frac{Y}{R} \text{ and } L(Y, R) = \gamma Y + \frac{\mu}{R}
$$

3

with positive parameters A, γ and μ. The conditions, $\dot{Y}(t) = \dot{R}(t) = \dot{M}(t) = 0$ determine the unique steady state (Y^*, R^*, M^*) such that

$$Y^* = \frac{g}{\tau}, \ R^* = \frac{A}{s(1-\tau)} \text{ and } M^* = \gamma Y^* + \frac{\mu}{R^*}. \tag{2}$$

Observing the facts that any economic system has delays in collecting tax and the length of such delay can be thought as the same for all agents in the same tax system, DS makes a simplified assumption that tax revenue at time t consists of two complementary components; one based on the current income and the other on past income,

$$T(t) = (1 - \varepsilon)\tau Y(t) + \varepsilon \tau Y(t - \theta) \tag{3}$$

where θ is a time delay and $\varepsilon < 1$ is a positive constant. Substituting (3) into (M_N) transforms the non-delay model into a fixed-delay model,

$$(M_F): \begin{cases} \dot{Y}(t) = \alpha \left(A \dfrac{Y(t)}{R(t)} - [s + (1-s)(1-\varepsilon)\tau]Y(t) + g - (1-s)\varepsilon\tau Y(t-\theta) \right), \\[2mm] \dot{R}(t) = \beta \left(\gamma Y(t) + \dfrac{\mu}{R(t)} - M(t) \right), \\[2mm] \dot{M}(t) = g - (1-\varepsilon)\tau Y(t) - \varepsilon\tau Y(t-\theta). \end{cases}$$

DS has already shown two main results, the existence of limit cycle through Hopf bifurcations and the co-existence of multiple cycles. In this section, we will show that the fixed delay model (M_F) gives rise a much wider variety of dynamic behavior including chaos.

The stationary state of the modified model (M_F) is the same as in the non-delay model, (Y^*, R^*, M^*). The linearized version of model (M_F) is

$$\begin{pmatrix} \dot{Y}_\delta(t) \\ \dot{R}_\delta(t) \\ \dot{M}_\delta(t) \end{pmatrix} = \begin{pmatrix} a_{11} & a_{12} & 0 \\ a_{21} & a_{22} & a_{23} \\ a_{31} & 0 & 0 \end{pmatrix} \begin{pmatrix} Y_\delta(t) \\ R_\delta(t) \\ M_\delta(t) \end{pmatrix} + \begin{pmatrix} -b_1 Y_\delta(t-\theta) \\ 0 \\ -b_2 Y_\delta(t-\theta) \end{pmatrix} \tag{4}$$

where the elements of the matrices are evaluated at the stationary point and given by

$$a_{11} = -\alpha(1 + (1-s)\varepsilon), \ a_{12} = -\alpha\frac{s^2(1-\tau)^2}{\tau A}g, \ a_{21} = \beta\gamma,$$
$$\tag{5}$$
$$a_{22} = -\beta\mu\frac{s^2(1-\tau)^2}{A^2}, \ a_{23} = -\beta, \ a_{31} = -(1-\varepsilon)\tau$$

and

$$b_1 = (1-s)\varepsilon\tau \text{ and } b_2 = \varepsilon\tau. \tag{6}$$

4

We also look for the exponential solutions, $Y_\delta(t) = e^{\lambda t} u$, $R_\delta(t) = e^{\lambda t} v$ and $M_\delta(t) = e^{\lambda t} w$, and substitute these into equation (4) to obtain the characteristic equation,

$$P(\lambda) + Q(\lambda)e^{-\lambda\theta} = 0 \tag{7}$$

where

$$P(\lambda) = \lambda^3 - (a_{11} + a_{22})\lambda^2 + (a_{11}a_{22} - a_{12}a_{21})\lambda - a_{12}a_{23}a_{31} \tag{8}$$

and

$$Q(\lambda) = b_1\lambda^2 - a_{22}\lambda + a_{12}a_{23}b_2. \tag{9}$$

If we introduce notation

$$p_2 = -(a_{11} + a_{22}), \ \ p_1 = a_{11}a_{22} - a_{12}a_{21}, \ \ p_0 = -a_{12}a_{23}a_{31}$$

and

$$q_2 = b_1, \ \ q_1 = -a_{22}, \ \ q_0 = a_{12}a_{23}b_2,$$

then equation (7) can be rewritten as

$$\lambda^3 + p_2\lambda^2 + p_1\lambda + p_0 + \left(q_2\lambda^2 + q_1\lambda + q_0\right) e^{-\lambda\theta} = 0. \tag{10}$$

Suppose that $\lambda = i\omega$, $\omega > 0$, is a root of this equation. Substituting it into the equation and then separating the real and imaginary parts, we have

$$-p_2\omega^2 + p_0 + (q_0 - \omega^2 q_2)\cos\theta + \omega q_1 \sin\omega\theta = 0$$
$$-\omega^3 + \omega p_1 + \omega q_1 \cos\omega\theta - (q_0 - \omega^2 q_2)\sin\omega\theta = 0. \tag{11}$$

Thus

$$(q_0 - \omega^2 q_2)^2 + (\omega q_1)^2 = (p_2\omega^2 - p_0)^2 + (\omega^3 - \omega p_1)^2.$$

Hence ω must be a positive root of the following equation

$$\omega^6 + (p_2^2 - 2p_1 - q_2^2)\omega^4 + (p_1^2 - 2p_0p_2 - q_1^2 + 2q_0q_2)\omega^2 + (p_0^2 - q_0^2) = 0.$$

Let $z = \omega^2$. Then the sextic equation can be reduced to a cubic equation,

$$\psi(z) = z^3 + az^2 + bz + c = 0 \tag{12}$$

with

$$a = p_2^2 - q_2^2 - 2p_1,$$

$$b = p_1^2 + 2q_0q_2 - 2p_0p_2 - q_1^2,$$

$$c = p_0^2 - q_0^2.$$

The discriminant of $\psi(z)$ is

$$D = a^2b^2 + 18abc - 4b^3 - 4a^3c - 27c^2.$$

$\psi(z)$ has one real root and a conjugate pair of imaginary roots if $D < 0$ and three distinct real roots if $D > 0$.[3] Notice that

$$p_0 - q_0 = \alpha\beta\frac{s^2(1-\tau)^2}{A}(1-2\varepsilon) \tag{13}$$

which is negative if $\varepsilon > 1/2$ and positive if $\varepsilon < 1/2$. The rest of this section is divided into two subparts: Dynamics in the case of $\varepsilon > 1/2$ is first considered and then in the case of $\varepsilon < 1/2$.

2.1 Delay tax is dominant: $\varepsilon > 1/2$

We take $\varepsilon = 3/5$ in this section.[4] Returning to equation (3), we see that more than half of the tax revenue is delayed when $\varepsilon > 1/2$. We specify the parameter values and formulate this specification as an assumption since we repeatedly use this specification of the parameters in numerical studies to be employed below.

Assumption $\alpha = \beta = A = 1$, $\gamma = 4/5$, $\mu = 3$, $s = 1/5$ and $\bar{g} = 10$.

Under Assumption, clearly $b > 0$ and $c < 0$ while it depends on a value of τ whether a is positive or negative. In Figure 1(A), the upward-sloping black curve is the $a = 0$ curve indicating that $a < 0$ to its left and $a > 0$ to its right. The sign of the discriminant is also τ-dependent. $D > 0$ in the light blue regions, $D < 0$ in the ocher region and $D = 0$ on their boundaries. Along the horizontal line at $g = \bar{g}$, three critical values of τ are determined so that the discriminant is zero. We denote them as τ_i for $i = 1, 2, 3$ in ascending order. The horizontal line also crosses the $a = 0$ curve at τ_a. Having the signs of a and D with respect to τ and then applying Descartes' rule, we can determine the number of positive roots along the horizontal line[5]:

(1) one positive root (and a pair of imaginary roots) if $0 < \tau < \tau_1$,
(2) three distinctive positive roots if $\tau_1 < \tau < \tau_2$,
(3) one positive root (and a pair of imaginary roots) if $\tau_2 < \tau < \tau_a$,
(4) one positive root (and a pair of imaginary roots) if $\tau_a < \tau < \tau_3$,
(5) one positive root (and two negative roots) if $\tau_3 < \tau < 1$.

Figure 1(B) illustrates how the number of the positive roots and the value of $\omega = \sqrt{z}$ depend on τ. A different color curve corresponds to a different root.

---

[3] Introducing a new variable, $x = z + a/3$, reduces $\psi(z)$ to the simplified form,

$$x^3 + px + q$$

in which the discriminant is

$$\left(\frac{q}{2}\right)^2 + \left(\frac{p}{3}\right)^2$$

and p and q are defined accordingly. We can arrive at the same results to be obtained even if this form of the discriminant is used.

[4] The results to be obtained in this section do not depend on the selection of the particular value of ε as far as $\varepsilon > 1/2$.

[5] In the same way, we can determine this number for any other value of g.

Solving $\psi(z) = 0$ yields at most three positive solutions, z_i for $i = 1, 2, 3$.[6] The red curve is associated to $\omega_1 = \sqrt{z_1}$, the blue curve to $\omega_2 = \sqrt{z_2}$ and the green curve to $\omega_3 = \sqrt{z_3}$. It can be seen that three different-color curves are illustrated for $\tau \in (\tau_1, \ \tau_2)$ and two different color curves are coincident for $\tau = \tau_1$ and $\tau = \tau_2$ when equation (12) has equal positive roots. Only one curve is illustrated for any other values of τ. We can summarize the results on the number of the positive roots and the associated purely imaginary roots of equation (12):

Proposition 1 *Given Assumption and $\varepsilon = 3/5$, there are three purely imaginary solutions, $\lambda_j = i\omega_j$ for $j = 1, 2, 3$ with $\omega_3 > \omega_2 > \omega_1 > 0$ if $\tau_1 < \tau < \tau_2$, two imaginary solutions with $\omega_3 = \omega_2 > \omega_1$ or $\omega_3 > \omega_2 = \omega_1$ if $\tau = \tau_1$ or $\tau = \tau_2$ and one imaginary solution $\lambda = i\omega_1$ if $\tau < \tau_1$ or $\lambda = i\omega_3$ if $\tau > \tau_2$.*

(A) Region division   (B) Real roots
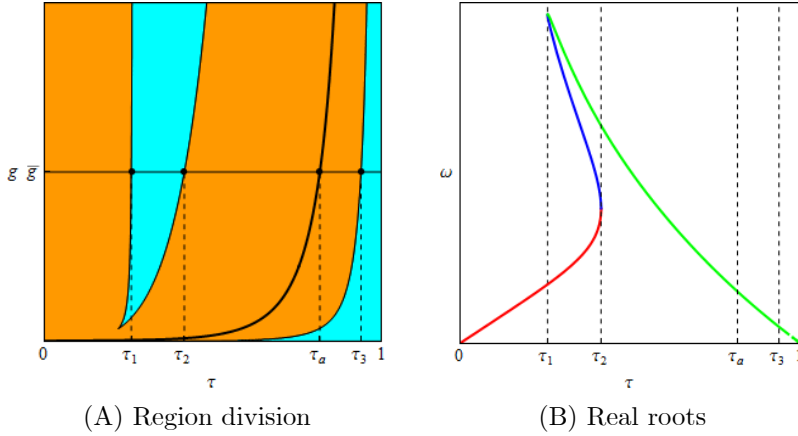
Figure 1. Positive roots of the characteristic equation (10)

From (11), we obtain two solutions

$$\sin \omega\theta = \omega \frac{\omega^4 q_2 - \omega^2(q_0 + p_1 q_2 - p_2 q_1) + p_1 q_0 - p_0 q_1}{(q_0 - \omega^2 q_2)^2 + (\omega q_1)^2},$$

$$\cos \omega\theta = \frac{\omega^4(q_1 - p_2 q_2) + \omega^2(p_0 q_2 + p_2 q_0 - p_1 q_1) - p_0 q_0}{(q_0 - \omega^2 q_2)^2 + (\omega q_1)^2}.$$

(14)

There is a unique value of $\omega\theta$, $0 < \omega\theta \leq 2\pi$ satisfying both equations. Taking an inverse of the second equation[7] and taking account of the fact that the cosine function has the same value for every 2π into account, the critical value of delay θ is determined as

$$\theta = \varphi(\tau, n)$$

---

[6] We do not give an explicit form of each z_i as it is long and complicated.
[7] Solving the first equation yields the same value of θ.

where $\varphi(\tau, n)$ is defined

$$\varphi(\tau, n) = \frac{1}{\omega} \left[\cos^{-1} \left(\frac{\omega^4(q_1 - p_2 q_2) + \omega^2(p_0 q_2 + p_2 q_0 - p_1 q_1) - p_0 q_0}{(q_0 - \omega^2 q_2)^2 + (\omega q_1)^2} \right) + 2n\pi \right] \tag{15}$$

for $n = 1, 2, \ldots$ Substituting a positive ω, which is functional for τ, into this equation determines the *partition curve* that partitions the (τ, θ) plane by separating the stable region of it from the unstable region. In Figure 2, the stationary state is locally stable in the yellow region and unstable in the white region. Thus the boundary between these regions is the boundary curve which consists of the segments of $\theta = \varphi(\tau, n)$ for $n = 0, 1$. The color of the partition curve is the same as the color of the positive root curve as depicted in Figure 1(B). The distorted L-shaped continuous curve with three different color segments is the partition curve with $n = 0$. Its lowest part colored in green crosses the horizontal axis twice at $\tau = \tau_A$ and $\tau = \tau_B$ and becomes negative between these intersections. So this captures the fact that if there is no delay (that is, $\theta = 0$), then the steady state is locally unstable for τ between these two values.[8] The two slender and deformed U-shaped curves having blue and green segments are the $\theta = \varphi(\tau, n)$ curves for $n = 1$ and $n = 2$, respectively. The $\theta = \varphi(\tau, n)$ curve shifts upward when the value of n increases.[9] Given the length of delay, the steady state loses stability for the tax rate on the boundary of the yellow region. Apparently such critical values of the tax rate are θ-dependent and different from τ_A, for which the steady state loses stability in the non-delay model.

Having determined the partition curves, we now examine the *delay effect* and the *tax effect* on stability. The former is caused by a change in the length of delay and is examined by changing θ along a vertical line at some τ. On the other hand, the latter is caused by a change in the tax rate with a positive delay

---

[8] More explanations are given later.

[9] The red segments with $n \geq 1$ have much larger θ and are located outside Figure 4.

8

and obtained by changing τ along a horizontal line at some θ.
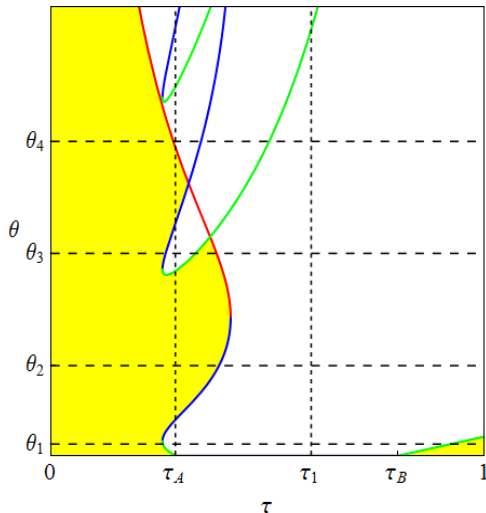
Figure 2. Partition curves with $\varepsilon > 1/2$

2.1.1 Tax Effect

We study the tax effect. Again as a bench mark, we first simulate the model (M_F) with $\theta = 0$ or the model (M_N) twice. Under Assumption, $\tau_A \simeq 0.29$ and $\tau_B \simeq 0.8$. The initial values of Y and R are the same in both simulations, $Y(0) = Y^*$ and $R(0) = R^*$ but the initial values of M are different, $M(0) = M^* + 1$ in the first simulation and $M(0) = M^* + 5$ in the second simulation, to verify the initial point dependency. The resultant bifurcation diagrams are presented in Figures 3(A) and 3(B), in each of which the downward sloping black curve depicts the equilibrium value of output, $Y^e = g/\tau$. In the simulations, the bifurcation parameter τ is increased from 0.2 to 1 with an increment of $1/1000$, the iterations are repeated 5000 times and the local maximum and minimum of $y(t)$ for the last 100 iterations are plotted against each value of τ. In Figure 3(A), the bifurcation diagram of the first simulation is depicted. It is observed that the stationary state loses stability when τ arrives at τ_A and bifurcates to a periodic cycle having one maximum and one minimum for $\tau > \tau_A$. It is also observed that the oscillation disappears at $\tau = \tau_B$ and stability is regained for $\tau > \tau_B$. In Figure 3(B), the bifurcation diagram in the second simulation is illustrated. It is seen that stability is lost at $\tau = \tau_A$ as in Figure 3(A) but regained at some value larger than τ_B. Further simulations with different initial points have been conducted and then lead to the fact that stability is regained not necessarily at $\tau = \tau_B$ but at some larger value although stability is always lost at $\tau = \tau_A$. These numerical results are summarized as follows:

Proposition 2 *Given Assumption, the non-delay model* (M_N) *generates periodic oscillations when the steady state is destabilized and has initial point dependency when it regains stability.*

(A) $m(0) = M^* + 1$

(B) $m(0) = M^* + 5$
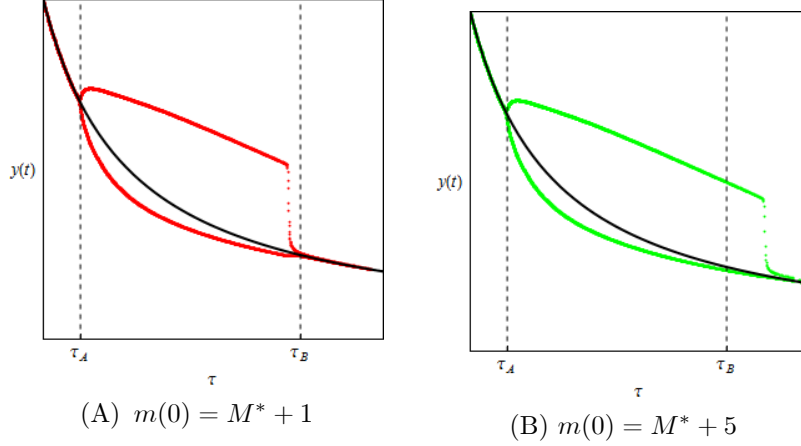
Figure 3. Bifurcation diagrams with different initial values

We now look into the case of positive delay to examine whether changing the value of the positive delay θ essentially affects the results obtained without delay. To this end, we perform simulations with four different values, $\bar{\theta}_1 = 0.5$, $\bar{\theta}_2 = 4$, $\bar{\theta}_3 = 9$, $\bar{\theta}_4 = 14$ and two different constant initial functions $\varphi_1(t) = M^* + 1$ and $\varphi_2(t) = M^* + 5$ for $t \leq 0$. We choose τ as the bifurcation parameter and increase its value from zero to unity along the horizontal dotted lines at $\theta = \theta_i$ for $i = 1, 2, 3, 4$ in Figure 2. Given θ_i, let τ^s denote the critical value of the tax rate for which the horizontal line at θ_i crosses the partition curve from left for the first time. The resultant bifurcation diagrams are given in Figures 4(A), 4(B), 4(C) and 4(D) where stability is lost for $\tau = \tau^s$ and the isoelastic black curve describes the equilibrium level of output. In each figures, the diagram with $\varphi_1(t)$ is colored in red, the one with $\varphi_2(t)$ in blue and the red diagram is superimposed on the blue diagram. The following results are obtained. There is no big difference between Figure 3 and Figure 4(A), the steady state loses stability at $\tau = \tau^s$, bifurcates to a limit cycle having one maximum and one minimum and regains stability at a value depending on the selection of the initial function. Figure 4(B) shows the birth of oscillations having several maxima and minima, indicating that the delay matters. Notice two issues: one is that the blue parts can be seen for larger values of τ being close to unity, implying that the selection of the initial function affects dynamics there; the other is that its effect is economically harmless because some parts of a time trajectory become negative (i.e., economically meaningless) when it is

effective. Figure 4(C) yields different dynamics. The steady state loses stability at $\tau = \tau_1^s$, regains it at $\tau = \tau_2^s$ and then loses stability again at $\tau = \tau_3^s$. As a result of a larger delay, oscillations for $\tau > \tau_3^s$ exhibit more ups and downs than those in Figure 4(B). In the final example, much more complicated oscillations are observed and dynamics becomes economically infeasible when becomes large as in Figure 4(D).

From these numerical simulations we obtain the following two results. First, different initial functions generate only limited effects on economically feasible dynamics having positive trajectories. In other words, the tax effect has only minor initial function dependency. Second, the shape differences among the bifurcation diagrams reveal that the tax effect with a large value of θ generates substantial effects on output dynamics. Concerning the stability switch, we find that there are two different ways. Stability loss and regain in the delay model occur for very small values of θ in the same way as in the non-delay model. The stability regain takes place only once for a relatively large value of τ. We notice in Figure 2 that the lower end of the U-shaped curve with $n = 1$ breaks into the stable yellow region and makes that region unstable. If a value of θ is appropriately selected such that a horizontal line at this θ crosses the lower part of the U-shaped curve, then increasing values of τ along this line induce stability switches three times for relatively smaller values of τ and finally destabilize the steady state. The results of numerical simulations are summarized as follows:

Proposition 3 *The tax effects substantially depend on the delay at least in three ways: (i) the delay model does not have a strong initial function dependency regardless of the length of delay; (ii) unstable trajectories exhibit more erratic ups and downs as the length of delay becomes longer; (3) stability switch can occur for some value of delay.*

(A) $\bar{\theta}_1 = 0.5$ (B) $\bar{\theta}_2 = 4$

(C) $\bar{\theta}_3 = 9$ (D) $\bar{\theta}_4 = 4$
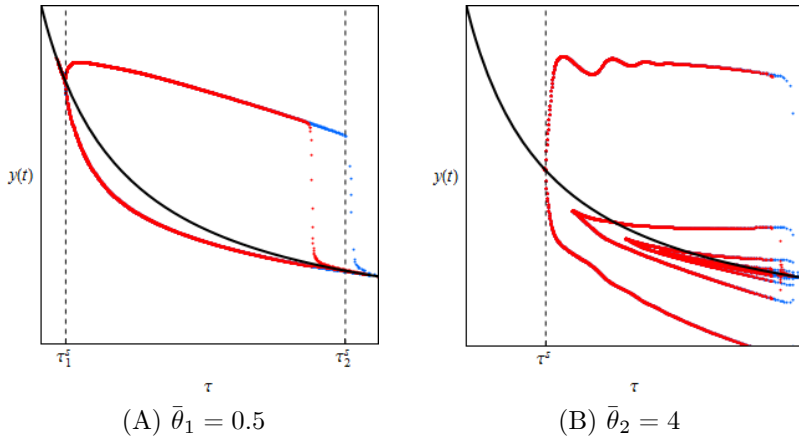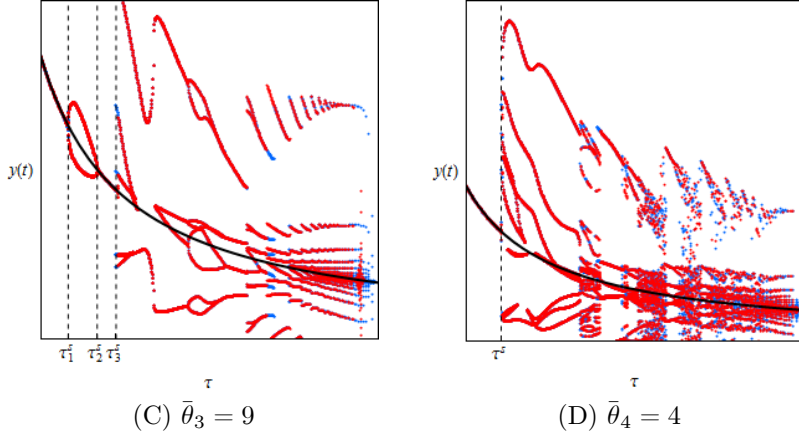
Figure 4. Bifurcation diagrams with respect to τ

2.1.2 Delay Effect

To verify the delay effects caused by changing the length of delay on stability, we select delay θ as the bifurcation parameter and examine the sign of the derivative of $Re[\lambda(\theta)]$ at the points where $\lambda(\theta)$ is purely imaginary. Differentiating equation (12) with respect to θ yields

$$\left(\frac{d\lambda}{d\theta}\right)^{-1} = -\frac{3\lambda^2 + 2p_2\lambda + p_1}{(\lambda^3 + p_2\lambda^2 + p_1\lambda + p_0)\lambda} + \frac{2q_2\lambda + q_1}{(q_2\lambda^2 + q_1\lambda + q_0)\lambda} - \frac{\theta}{\lambda}$$

where we study, only for convenience, the inverse of $d\lambda/d\theta$. Substituting $\lambda = i\omega$, rationalizing the denominator and noticing that the terms with λ and λ^3 are imaginary while the constant and the terms with λ^2 and λ^4 are real yield the following form of the real part of the derivative of λ:

$$\text{Re}\left[\left(\frac{d\lambda}{d\theta}\right)^{-1}\bigg|_{\lambda=i\omega}\right] = \frac{\psi'(\omega^2)}{\omega^2(\omega^2 - p_1)^2 + (p_2\omega^2 - p_0)^2}$$

where the denominator is definitely positive. It is seen that the sign of the real part is positive for ω_i with $\psi'(\omega^2) > 0$ and negative for ω_i with $\psi'(\omega^2) < 0$. Indeed, it can be verified that if equation $\psi(\omega^2) = 0$ has three positive roots, ω_1, ω_2, ω_3, then the derivative of the root has the following directions of inequality:

$$\text{Re}\left[\frac{d\lambda}{d\theta}\bigg|_{\lambda=i\omega_1}\right] > 0, \ \text{Re}\left[\frac{d\lambda}{d\theta}\bigg|_{\lambda=i\omega_2}\right] < 0, \text{and} \ \text{Re}\left[\frac{d\lambda}{d\theta}\bigg|_{\lambda=i\omega_3}\right] > 0 \qquad (16)$$

and otherwise $\psi(\omega^2) = 0$ has only one positive root with

$$\mathrm{Re}\left[\frac{d\lambda}{d\theta}\bigg|_{\lambda=i\omega}\right] > 0. \tag{17}$$

The positive sign implies that all roots cross the imaginary axis from left to right as θ increases, that is, stability is lost. On the other hand, the negative sign means crossing the axis in the reverse direction, that is, stability is gained. We now perform two simulations with different values of τ. In the first simulation, we increase θ from zero to 20 along the vertical dashed line at $\tau = \tau_A(\simeq 0.287)$ in Figure 2. The vertical line crosses the $\theta = \varphi(\tau, n)$ $(n = 0, 1, 2)$ curves six times. Three intersections with the lower, middle and upper blue curves are at $\theta_1 \simeq 1.59$, $\theta_4 \simeq 13.7$ and $\theta_6 \simeq 19.1$. Similarly two intersections with the middle and upper green curves are at $\theta_2 \simeq 8.23$ and $\theta_5 \simeq 16.4$. Finally $\theta_3 \simeq 10.3$ is the intersection with the red curve. The subscripts of θ_i are labeled in the ascending order. Numerical result is illustrated in Figure 5(A). The starting point of $\tau = \tau_A$ and $\theta = 0$ is on the lowest green segment so that the real part of the eigenvalue is zero and its derivative with respect to θ is positive. The steady state loses stability when θ becomes positive and bifurcates to a periodic cycle. As the length of delay becomes larger, the cycle expands, shrinks and then merges with the stationary state at $\theta = \theta_1$ to gain stability. It loses stability again when increasing θ crosses the green partition curve from below at $\theta = \theta_2$. Repeating the same process, the steady state regains stability at $\theta = \theta_3$. The second switch from instability to stability occurs. Passing through a small stability interval of θ, the steady state is destabilized when increasing θ arrives at the downward-sloping red partition curve at $\theta = \theta_4$. For $\theta > \theta_4$, the steady state remains unstable and a periodic cycle with seven extremal values emerges.

In the second simulation, τ is increased to $\tau_1 = 0.6$. As seen in Figure 2, the dotted vertical line at $\tau = \tau_1$ does intersect with the partition curve and the steady state is locally unstable even at $\theta = 0$. Comparing Figure 5(A) with Figure 5(B) implies that fluctuations becomes complicated as θ increases. Period-doubling and period-halving bifurcations can be observed. Although complex fluctuation emerges for a larger value of θ, its time trajectory in the gray region of Figure 5(B) takes negative value. Notice that the difference between these two simulations is only the value of τ. We summarize the results:

Proposition 4 *Delay affects output dynamics and generates a shape different bifurcation cascade depending on the value of the tax rate.: (1) when a smaller value of the tax rate is given, increasing θ finally destabilizes the steady state after repeating several stability switches; (2) when a larger value of the tax rate is given, no stability switch occurs and trajectories exhibit more ups and downs as θ increases*

13

(A) $\tau = \tau_A(\simeq 0.287)$ (B) $\tau = \tau_1(= 0.6)$
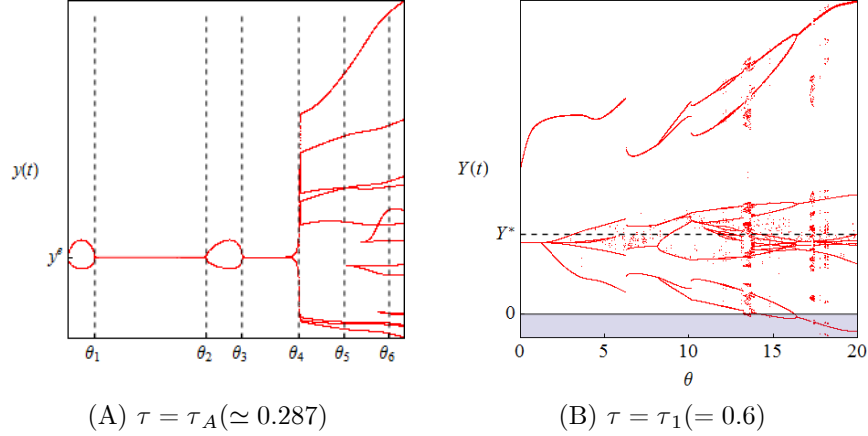
Figure 5. Bifurcation diagrams with respect to θ

2.2 Current tax is dominant: $\varepsilon < 1/2$

In this section we take $\varepsilon = 2/5$ and consider the case where non-delay tax is dominant over delay tax.[10] For $\varepsilon = 2/5$, $c > 0$ always, however, the signs of a, b and D are ambiguous. In Figure 6(A), the loci of $a = 0$ and $b = 0$ are illustrated in red and blue and both are upward-sloping. It can be checked that $a > 0$ and $b < 0$ to the right of the corresponding locus and the inequality is reversed to the left. The $D = 0$ locus is depicted in black and takes a L-shaped curve. $D > 0$ in the light-blue region to the right of the locus and $D < 0$ in the yellow region to the left. Along the $g = \bar{g}$ horizontal line, three critical values of τ, $\tau_a \simeq 0.63$, $\tau_b \simeq 0.49$ and $\tau_D \simeq 0.27$, are obtained so that $a = 0$, $b = 0$ and $D = 0$, respectively. Applying Descartes' rule of signs, we can determine the number of positive roots along this horizontal line according to the signs of these parameters and the discriminant:

(1) no positive roots if $\tau < \tau_D$,
(2) two positive roots (and one negative root) if $\tau_D < \tau \leq \tau_b$,
(3) two positive roots (and one negative root) if $\tau_b < \tau \leq \tau_a$,
(4) two positive roots (and one negative root) if $\tau_a < \tau < 1$

where the two positive roots are equal for $\tau = \tau_D$. Dependency of the two roots $\omega_i = \sqrt{z_i}$ $(i = 1, 2)$ on the value of the tax rate is described by the blue and green downward sloping curves shown in Figure 6(B). We summarize the results as follows:

---

[10] As in the previous case, this particular value is selected only for convenience. We could have the qualitatively same results with different values of ε as far as $\varepsilon < 1/2$.

14

Proposition 5 *Given Assumption, there are two purely imaginary solutions, $\lambda_i = i\omega_i$ for $i = 1, 2$ with $\omega_2 > \omega_1 > 0$ if $\tau > \tau_D$ (or $D > 0$) and no imaginary solutions if $\tau < \tau_D$ (or $D < 0$).*

(A) Region division   (B) Real roots with $\bar{g} = 10$
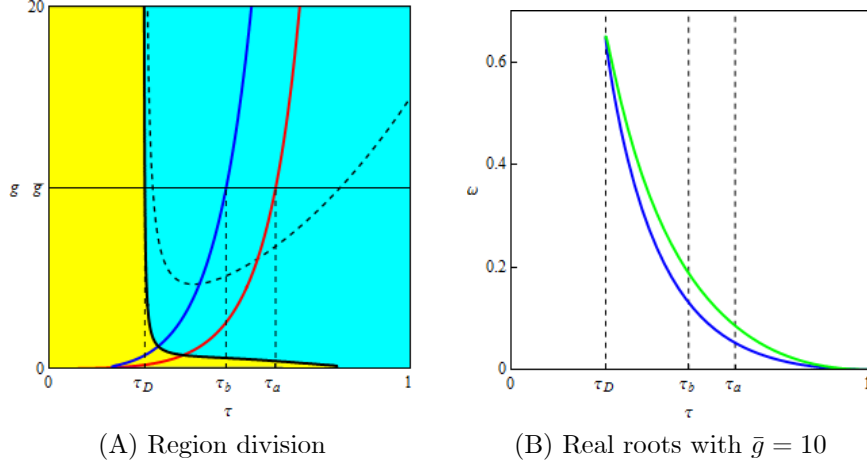
Figure 6. Positive roots of characteristic equation (12) with $\varepsilon = 2/5$

Similarly to the case of $\varepsilon = 3/5$, we can obtain the partition curves in the (τ, θ) plane by substituting ω_i ($i = 1, 2$) into equation (15). Five distorted U-shaped curves for $n = 0, 1, 2, 3, 4$ are depicted in Figure 7 where the steady state is asymptotically stable in the yellow region. Since the curve shifts upward as n increases, the lowest curve is with $n = 0$ and the highest curve with $n = 4$. Each curve consists of blue and green segments associated with two positive roots with the same color in Figure 6(B). For $\tau < \tau_D$, the steady state is locally asymptotically stable irrespective of the length of delay. Since delay does not affect dynamics, such delay is called *harmless*. For $\tau > \tau_D$, a significant change in the stability region takes place. The boundary of the stability region is made up of infinitely many arcs of the partition curves. The most remarkable effect of the change is that as the delay θ is increased, many stability switches may occur for a fixed value of τ, especially for τ closer to τ_D. This is in sharp contrast with the case of $\varepsilon > 1/2$ where, after several stability switches, further increased in value of θ could not induce re-stabilization of the steady state when it crosses the red segment of the partition curve shown Figure 2.
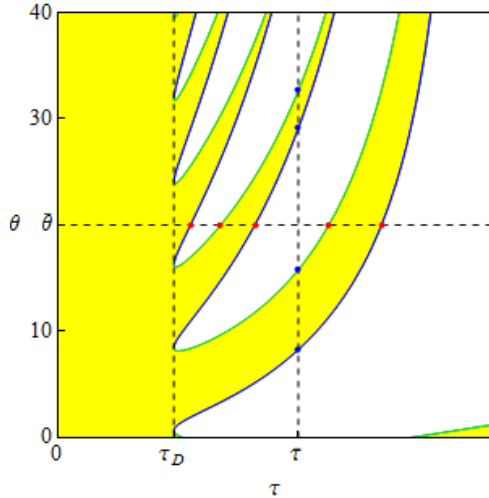
Figure 7. Partition curves with $\varepsilon = 2/5$

In order to study the global stability properties of the steady state, we first fix the parameter values, $\bar{\theta} = 20$ and $\bar{\tau} = 0.55$ and then perform two numerical simulations.[11] In the first simulation, we examine the tax effect with positive delay by increasing τ from zero to unity along the horizontal dotted line at $\theta = \bar{\theta}$. The bifurcation diagram with respect to τ is illustrated in Figures 8(A) where stability is regained twice indicating that the tax rate affects the stability as well as the instability. It is observed that unstable trajectories converge to periodic cycles whose periodicity increases as the tax rate becomes larger. Period-doubling and -halving process are also observed for $\tau \in (\tau_3, \tau_4)$. In the second simulation, we detect the delay effect by increasing θ from zero to 40 along the vertical dotted line at $\tau = \bar{\tau}$. The bifurcation diagrams with respect to θ is illustrated in Figure 8(B) where the delay effect seems to be similar to the delay tax effect. Indeed, stability switches take place twice and unstable trajectories exhibit simple dynamics for smaller values of θ, period-doubling and period-halving occur for medium values (i.e., $\theta \in (\theta_2, \theta_3)$) and complex dynamics emerges for larger values (i.e., $\theta > \tau_3$).

Proposition 6 *Given Assumption and $\omega = 2/5$, delay model has multiple stability switches and can generate simple dynamics to complex dynamics as the bifurcation parameter (τ or θ) becomes larger.*

---

[11] Since it is verified that the initial function dependency is weak, we take the same initial function, $\varphi(t) = M^* + 1$, in both simulations.

(A) Tax effect ($\theta = 20$)   (B) Delay effect ($\tau = 0.55$)
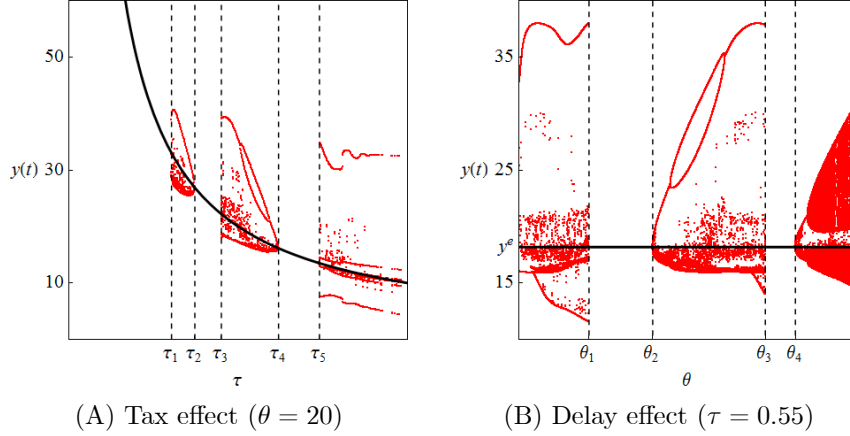
Figure 8. Bifurcation diagrams

3 Distributed Delay IS-LM Model

As mentioned in the Introduction, FM concerns the situation where there is a wide variation in collecting tax due to heterogenous economic agents. FM replaces the fixed delay in tax collection with distributed delay and show occurrence of chaotic oscillations. It adopts a very special form of tax collection, $T(t) = \tau Y^e(t)$ where $Y^e(t)$ is the expected income at time t and is a weighted average of past incomes. We reconsider the FM version of the IS-LM model augmented with the continuously distributed time delay. Our version is different in the following two points. First, the general form of tax collection given in equation (3), $T(t) = (1-\varepsilon)\tau Y(t) + \varepsilon\tau Y^e(t)$, is assumed, which includes the special form when $\varepsilon = 1$. Second, we use a bell-shaped delay kernel instead of the exponentially declining delay kernel. Fixed delay model (M_F) is now modified as a distributed delay model,

$$(M_D): \begin{cases} \dot{Y}(t) = \alpha\left(A\dfrac{Y(t)}{R(t)} + g - (s + (1-s)(1-\varepsilon)\tau Y(t) - (1-s)\varepsilon\tau Y^e(t)\right) \\[2mm] \dot{R}(t) = \beta\left(\gamma Y(t) + \dfrac{\mu}{R(t)} - M(t)\right) \\[2mm] \dot{M}(t) = g - (1-\varepsilon)\tau Y(t) - \varepsilon\tau Y^e(t) \end{cases}$$

with

$$Y^e(t) = \int_0^t W(t - \eta, \theta, m)Y(\eta)d\eta$$

17

where the weighting function or the delaying kernel is defined by

$$W(t - \eta, \theta, m) = \begin{cases} \dfrac{1}{\theta} e^{-\frac{1}{\theta}(t-s)} & \text{if } m = 0, \\[3mm] \dfrac{1}{m!} \left(\dfrac{m}{\theta}\right)^{m+1} (t-\eta)^m e^{-\frac{m}{\theta}(t-s)} & \text{if } m \geq 1. \end{cases} \tag{18}$$

Here m is a nonnegative integer and θ is a positive real parameter, which corresponds to the average length of delay. The expected output formed at time t is the weighted average of the actual demand in the past. According to definition (18), the shape of the weighting function is determined by the value of the shape parameter m. For $m = 0$, weights are exponentially declining with the most weight given to the most current data (i.e., a fading memory). FM confines attention to this case and show that the distributed delay IS-LM model can display stability switch from stability to instability through a Hopf bifurcation and gives rise to chaotic motions when the average length of the delays is relatively large. For $m \geq 1$, zero weight is given to the most current data, rising to maximum as $\eta = t - \theta$ and declining exponentially thereafter. Thus the weights take a bell-shaped form which becomes taller and thinner as m increases. We draw attention mainly to the case with $m \geq 1$.

To examine the local stability of this dynamical system in a neighborhood of the steady state, we linearize the model to relate it to the relevant parameters. We start with the case of $m = 1$ in which the expected output is

$$Y^e(t) = \int_0^t \left(\frac{1}{\theta}\right)^2 (t - \eta) e^{-\frac{1}{\theta}(t-s)} Y(\eta) d\eta$$

and its rate of change is

$$\dot{Y}^e(t) = \frac{1}{\theta} \left(X(t) - Y^e(t)\right). \tag{19}$$

Here the new variable $X(t)$ is defined as

$$X(t) = \int_0^t \frac{1}{\theta} e^{-\frac{1}{\theta}(t-s)} Y(\eta) d\eta$$

and its time derivative is

$$\dot{X}(t) = \frac{1}{\theta} \left(Y(t) - X(t)\right). \tag{20}$$

Adding differential equations (19) and (20) to the integro-differential system (M_D) yields a 5D dynamical system of ordinary differential equations. Its Jacobi matrix is

$$\boldsymbol{J}_{m=1} = \begin{pmatrix} a_{11} & a_{12} & 0 & -b_1 & 0 \\ a_{21} & a_{22} & a_{23} & 0 & 0 \\ a_{31} & 0 & 0 & -b_2 & 0 \\ 0 & 0 & 0 & -\frac{1}{\theta} & \frac{1}{\theta} \\ \frac{1}{\theta} & 0 & 0 & 0 & -\frac{1}{\theta} \end{pmatrix}$$

where a_{ij} and b_i are the same as those given in (5) and (6), respectively. Expanding $\det(\boldsymbol{J}_{m=1} - \lambda \boldsymbol{I}) = 0$ yields the characteristic equation of the Jacobi matrix $\boldsymbol{J}_{m=1}$,

$$P(\lambda)\left(1 + \frac{\lambda\theta}{1}\right)^{1+1} + Q(\lambda) = 0,$$

where $P(\lambda)$ and $Q(\lambda)$ are already given in (8) and (9). In the same way, the characteristic equations with $m = 2$ and $m = 3$ are obtained as

$$P(\lambda)\left(1 + \frac{\lambda\theta}{2}\right)^{2+1} + Q(\lambda) = 0 \text{ and } P(\lambda)\left(1 + \frac{\lambda\theta}{3}\right)^{3+1} + Q(\lambda) = 0.$$

By induction, the characteristic equation has the general form

$$P(\lambda)\left(1 + \frac{\lambda\theta}{m}\right)^{m+1} + Q(\lambda) = 0,$$

which is an $(m+4)$-th order polynomial equation

$$a_0\lambda^{m+4} + a_1\lambda^{m+3} + ... + a_{m+3}\lambda + a_{m+4} = 0$$

where the coefficients a_i are defined accordingly.

3.1   Stability Analysis

Since it is difficult to obtain a general solution of the $(m+4)$-th degree characteristic equation, we confine attention to special cases with $m = 1, 2, 3$ and $m \to \infty$. We will analytically consider local stability of the steady state and then numerically examine global dynamics. Before proceeding to stability analysis, we construct the Routh-Hurwitz determinant:

$$J_m = \det \begin{pmatrix} a_1 & a_0 & 0 & 0 & \cdots & 0 \\ a_3 & a_2 & a_1 & a_0 & \cdots & 0 \\ a_5 & a_4 & a_3 & a_2 & \cdots & 0 \\ a_7 & a_6 & a_5 & a_4 & \cdots & 0 \\ . & . & . & . & \cdots & 0 \\ 0 & 0 & 0 & 0 & \cdots & a_{m+4} \end{pmatrix}.$$

Let J_m^k denote the k-th order leading principal minor of J_m.

In the case of $m = 1$, the characteristic function is a 5th degree polynomial and its coefficients are numerically confirmed to be all positive for $0 \le \varepsilon \le 1$

and $0 \leq \tau \leq 1$ under Assumption,

$$a_1 = \frac{50 + \theta(3 + (19 - 20\varepsilon)\tau + 3\tau^2)}{25\theta} > 0,$$

$$a_2 = \frac{125\tau + 10\theta\tau(3 + (19 - 20\theta)\tau + 3\tau^2) + \theta^2(1 - \tau)^2(40 + 3(5 - 4\varepsilon)\tau^2)}{125\theta^2\tau} > 0,$$

$$a_3 = \frac{50(1 - \varepsilon)\theta^2(1 - \tau)^2\tau + 5\tau(3 + 19\tau + 3\tau^2) + 2\theta(1 - \tau^2)(40 + 3(5 - 4\varepsilon)\tau^2)}{125\theta^2\tau} > 0,$$

$$a_4 = \frac{(1 - \tau)^2(8 + 20(1 - \varepsilon)\theta\tau + 3\tau^2)}{25\theta^2\tau} > 0,$$

$$a_5 = \frac{2(1 - \tau)^2}{5\theta^2} > 0,$$

where $a_0 = 1$. Furthermore it is also numerically verified that $\varepsilon = 3/5$ and $\varepsilon = 2/5$

$$J_1^2 = \det \begin{pmatrix} a_1 & a_0 \\ a_3 & a_2 \end{pmatrix} > 0 \text{ and } J_1^3 = \det \begin{pmatrix} a_1 & a_0 & 0 \\ a_3 & a_2 & a_1 \\ a_5 & a_4 & a_3 \end{pmatrix} > 0.$$

Notice that $J_1^4 > 0$ implies $J_1^5 > 0$ since $a_5 > 0$. So, according to the Routh-Hurwitz stability criterion, the following determinant needs to be positive for preserving local stability,

$$J_1^4 = \det \begin{pmatrix} a_1 & a_0 & 0 & 0 \\ a_3 & a_2 & a_1 & a_0 \\ a_5 & a_4 & a_3 & a_2 \\ 0 & 0 & a_5 & a_4 \end{pmatrix}.$$

Under the set of parameters given in Assumption, the $J_1^4 = 0$ locus is the partition curve. In Figures 9(A) and 9(B), the partition curves with $\varepsilon = 3/5$ and $\varepsilon = 2/5$ correspond to the right most curves arrowed by $m = 1$, respectively. The steady state is locally stable to the left of the curve and unstable to the right (i.e., the white region). Two other curves are the loci of $J_2^5 = 0$ and $J_3^6 = 0$, that is, the partition curves with $m = 2$ and $m = 3$. The yellow regions are the stability regions under the fixed time delay.[12] From these numerical examples, we obtain the following three results. The first is that the distributed time delay models are more stable than the fixed delay model in the sense that the stability region of the former is larger than the one of the latter. The partition curve shifts leftward as m becomes larger, shrinking the stable region. So the second result is that increasing the value of m has a destabilizing effect. The third is that different values of the weight ε between the current and past taxes do not

---

[12] In Figure 9(A), only the locus of $\theta = \varphi(\tau, n)$ for $n = 0$ is depicted for graphical convenience.

generate qualitatively different dynamics as is seen in Figures 9(A) and 9(B).

(A) $\varepsilon = 3/5$ (B) $\varepsilon = 2/5$
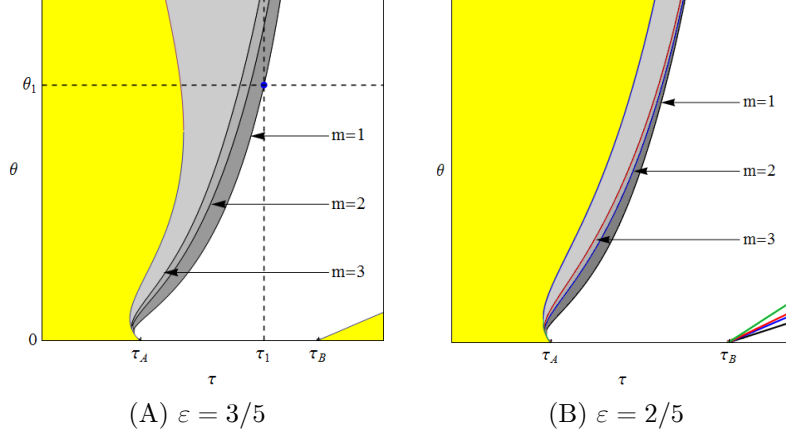
Figure 9. Region division and partition curves

The stable region with distributed delay becomes smaller as the value of m increases and converges to the region defined by the fixed delay when m tends to infinity. This result is natural if we notice the properties of the delay kernel. The kernel with $m \geq 1$ is bell-shaped and becomes more peaked around $t - \eta$ as m increases. Furthermore it tends to the Dirac delta function if $m \to \infty$. In consequence, for sufficiently large values of m, the delay kernel may be regarded as very close to the Dirac delta function and the dynamic behavior under the distributed delay is very similar to that under the fixed delay. We may explain this result mathematically by noticing that the characteristic equation with continuous delay can be written as

$$P(\lambda) + Q(\lambda) \left(1 + \frac{\theta \lambda}{m} \right)^{-(m+1)} = 0.$$

If m tends to infinity, then the left hand side converges to

$$P(\lambda) + Q(\lambda) e^{-\theta \lambda} = 0$$

which is identical with the characteristic equation (7) of the delay differential equation with a single fixed delay.[13] In short, under distributed delay, although we comprehensively use all delayed or past output data, the stability domain is sensitive to the shape of the delay kernel.

Proposition 7 *Increasing the value of the shape parameter m has a destabilizing effect in the sense that it decreases the stability region of the distributed*

---

[13] Notice that the same notation θ is used to describe the delay in the fixed and distributed models.

delay model, and $m \to \infty$ makes the distributed delay model converge to the fixed delay model.

Taking $\varepsilon = 3/5$, we conduct the final simulations of the delay and tax effects in the distributed model. In the first example, we increases the value of θ, the length of delay, from 0 to 10 along the dotted vertical line at $\tau = \tau_1$ that crosses the partition curve with $m = 1$ for $\theta = \theta_1$ in Figure 9(A). Figure 10(A) depicts a bifurcation diagram with respect to θ, in which cyclic oscillations around the unstable steady state emerge for $\theta < \theta_1$, the steady state regains stability at $\theta = \theta_1$ and is locally asymptotically stable for $\theta > \theta_1$. In the second example, we increase the value of τ, to verify the tax effect, along the dotted horizontal line at $\theta = \theta_1$ that crosses the partition curve with $m = 1$ for $\tau = \tau_1$. As seen in Figure 10(B), the steady state loses stability on the partition curve and bifurcates to cyclic oscillations for $\tau > \tau_1$.

(A) Delay effect ($\tau = 0.55$)   (B) Tax effect ($\theta = 20$)
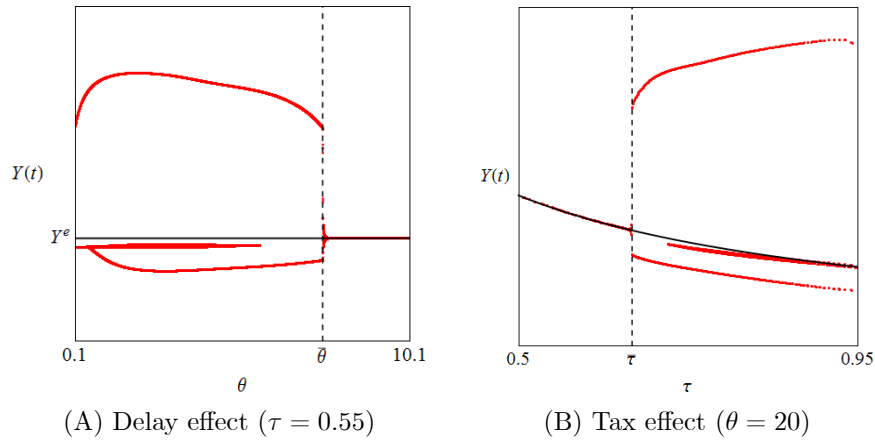
Figure 10. Bifurcation diagrams with $\varepsilon = 3/5$

4   Concluding Remark

Dynamic IS-LM model was considered with fixed and continuously distributed delays in past income. The non-delay model generates periodic oscillations with respect to the tax rate when the steady state loses stability and has initial point dependency when stability is regained. If the delay is fixed and its length is the bifurcation parameter, then the dynamic properties depend on whether the current tax is dominant or not. If it is, then the model has multiple stability, switches and can generate simple dynamics to complex dynamics as the bifurcation parameter increases. If not, then multiple stability switches occur and finally further increase leads to instability. If the delay is continuously distributed, then the stability region decreases as the shape parameter m of the

weighting function increases, and as $m \to \infty$, it converges to the stability region of the fixed delay model.

The existence of fixed and continuously distributed delays or multiple fixed or continuously distributed delays can be examined in a similar manner, however both the analytical study and the numerical simulations could become more complicated.

References

[1] Bellman, R. and Cooke, K. L. *Differential-difference Equations*. Academic Press, New York, 1956.

[2] Cushing, J., *Integro-differential Equations and Delay Models in Population Dynamics,* Springer-Verlag, Berlin/Heidelberg/New York, 1977.

[3] De Cesare, L. and Sportelli, M., A Dynamic IS-LM Model with Delay Taxation Revenues, *Chaos, Solitions and Fractals*, 25, 233-244, 2005.

[4] Fanti, L. and Manfredi, P., Chaotic Business Cycles and Fiscal Policy: An IS-LM Model with Distributed Tax Collection Lags, *Chaos, Solitions and Fractals*, 32, 736-744, 2007.

[5] Gandolfo, G., *Economic Dynamics*, 4th Edition, Springer-Verlag, Berlin/Heidelberg/ New York, 2010.

[6] Goodwin, R. The Nonlinear Accelerator and the Persistence of Business Cycles, *Econometrica* 19, 1-17, 1951.

[7] Kalecki, M., A Macrodynamic Theory of Business Cycles, *Econometrica*, 3, 327-344, 1935.

[8] Matsumoto, A. and Szidarovszky, F., Dynamics in an IS-LM model augmented with Fixed and Distributed Time Delays, mimeo, 2013.

[9] Sasakura, K., On the Dynamic Behavior of Schinasi's Business Cycle Model, *Journal of Macroeconomics*, 16, 423-444, 1994.

[10] Schinasi, G., A Nonlinear Dynamic Model of Short Run Fluctuations, *Review of Economic Studies*, 48, 649-659, 1981.

[11] Schinasi, G., Fluctuations in a Dynamic, Intermediate-run IS-LM model: Applications of the Poincare-Bendixon Theorem, *Journal of Economic Theory*, 28, 369-375, 1982.